

# Diffraction-free propagation of subwavelength light beams in layered media

Juan J. Miret<sup>1</sup> and Carlos J. Zapata-Rodríguez<sup>2,\*</sup>

<sup>1</sup>*Departamento de Óptica, Universidad de Alicante, P.O. Box 99, Alicante, Spain*

<sup>2</sup>*Departamento de Óptica, Universidad de Valencia, Dr. Moliner 50, 46100 Burjassot, Spain*

\*Corresponding author: carlos.zapata@uv.es

Received December 24, 2009; revised May 4, 2010; accepted May 7, 2010;  
posted May 25, 2010 (Doc. ID 122014); published June 18, 2010

Self-collimation of tightly localized laser beams demonstrated in periodic media relies on a perfect-matched rephasing of the Fourier constituents of the wavefield induced by a plane isofrequency curve. An alternate way paved for the achievement of such a phase matching condition developed a suitable spatial filtering in order to select those frequencies experiencing the same phase velocity projected over a given orientation. In principle this procedure is valid for complex structured metamaterials. However, a great majority of studies have focused on free-space propagation leading to the well-known Bessel beams. This paper is devoted to the analysis of this sort of nondiffracting beams traveling in one-dimensional metallic-dielectric photonic crystals. Specifically we present a family of localized radiation modes in multilayered periodic media, where in-phase superposition of  $p$ -polarized waves leads to radiative confinement around the beam axis. Excitation of surface plasmon polaritons yields an enhanced localization normally to the interfaces. Subwavelength beam widths along an infinitely long distance might potentially be obtained. © 2010 Optical Society of America

OCIS codes: 240.6680, 350.5500.

## 1. INTRODUCTION

Diffraction broadening is a natural process of electromagnetic fields involving an increment of the beam width as it propagates in free space. A geometrical light pencil necessarily evolves to a diverging wave in the Fraunhofer region, where the spot size increases linearly upon the longitudinal spatial coordinate. Initially, resistance to beam spreading is maintained within the so-called Rayleigh range [1], which is a parameter extensively employed in Gaussian laser beams estimating the boundaries of the near-field region. In the case of wavefields with diffraction-limited spot sizes, the Rayleigh range becomes extremely low approaching a wavelength. In the field of optics, however, it is demanded more robust systems capable of circumventing the diffraction phenomenon for innovative applications including electromagnetic tweezers [2], optical acceleration of charged particles [3], superlensing [4], optical interconnectors, and communications in general [5].

The transformation of a collimated beam of light into a diverging spherical wave may be explained in a simple way by using the plane-wave Fourier expansion of a wavefield. The evolution of each spectral component leads to a characteristic phase shift reaching a maximum value for the associated plane wave propagating along the beam axis. If the observation is performed at sufficiently short distances, dephasing between different elements in the spatial spectrum may be neglected. Therefore the transverse pattern is nearly undistorted resulting in the conservation of the beam size. Out of the near-field region, however, the effect of angular dispersion is clearly manifested, which yields a change in the transverse pattern and also a linear growth of the beam size.

Bearing in mind that phase shifts of the transverse spatial spectrum are governed by the dispersion equation, one may manage dephasing by tailoring the characteristic isofrequency contours of the medium. In particular, plane dispersion curves would lead to zero dephasing of the spectral elements of the field, and in principle the Rayleigh range would be infinitely enlarged along the normal direction of the dispersion surface. Photonic crystals are optical anisotropic media providing complex isofrequency curves with either positive or negative curvature. An appropriate choice of materials and lattice geometry would lead to flat dispersion curves with a zero Gaussian curvature along a given orientation [6–8]. This refers to the well-known canalization regime, which is favorable to minimize dephasing of the transverse spectrum, increasing the Rayleigh range of wavefields in comparison with free-space propagation. Experimental evidence of laser beams propagating in periodic media in the canalization regime for applications in nano-circuitry is reported elsewhere [9,10].

An alternate route consists of exciting spectral components all evolving with the same phase shift [11,12]. In free space this may be achieved by using a conical lens [13] or a Fabry–Perot etalon [14]. The resulting wavefield propagates, for instance, along the  $z$ -axis gaining a linear phase shift  $\exp(i\beta z)$  in the same manner than a plane wave. However, the propagation constant  $\beta > 0$  is lower (higher) than the wave number  $2\pi/\lambda$  for normal (negative) dispersion, and the transverse field cannot remain having a uniform profile. Bessel beams [15–17] are a well-known family of wavefields that belong to this kind, which hold a particular interest due to radial symmetry of the transverse intensity patterns and the strong field lo-

calization around the centered *focus* (say  $r=0$ ). As a consequence, the beam of light seems to violate the principle of diffraction as the bright spot propagates in a homogeneous dielectric medium maintaining a narrow waist without stretching.

The concept of diffraction-free propagation is also attractive if light travels in complex structured media. Nondiffracting beams with a Bessel profile may be found in stratified media if the unit vector ( $\mathbf{n}$ ) normal to the interfaces lies along the  $z$ -axis leading to normal incidence of the wavefield [18–21]. However, out-of-plane excitation cannot support the invariant propagation of Bessel beams [22]. For example, assuming that the medium is periodic, the elements of any Fourier superposition are necessarily Bloch modes leading to a significant asymmetry in the resultant pattern. Provided the projection  $\beta$  of the Bloch wave vector along the propagation direction coincides for every spectral component, we may have a nondiffracting localized beam if, additionally, the phase matching condition is satisfied [23]. This is also reported in two-dimensional photonic crystals [24,25].

In this paper we study the formation of localized waves which propagation is resonantly sustained on a given interface from a one-dimensional periodic metallo-dielectric medium. The surface resonance arises in transverse-magnetic (TM) waves ( $\mathbf{H} \perp \mathbf{n}$ ) provided the sign of the dielectric constant changes abruptly at both sides of the interface. The excitation of such surface plasmon polaritons (SPPs) is attained at comparatively high values of  $\beta$ , however, leading to a subwavelength beam size. In spite of such an extreme wave localization, the transverse pattern of the excited field in the linear medium, and so its beam width, is ideally maintained for infinitely long distances.

## 2. IN-PLANE PROPAGATION OF DIFFRACTION-FREE BEAMS IN METALLO-DIELECTRIC LAYERED MEDIA

Let us consider a monochromatic nondiffracting beam propagating in a multilayered medium. The  $y$ -axis is set such that it is perpendicular to the surfaces separating the metallic media and the adjacent dielectric media so that  $\mathbf{n}=\hat{\mathbf{y}}$ . In Fig. 1 we show schematically the multilayered system. The width of a metallic slab is  $w$ , with an element periodically replicated at a distance  $p$  along the

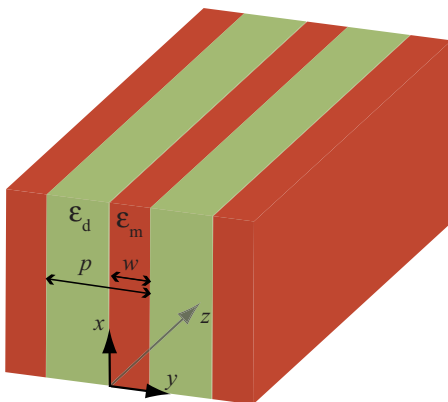


Fig. 1. (Color online) Schematic geometry of the planar-nano-layer-based medium.

$y$ -axis. We also assume that beam propagation is directed along the  $z$ -axis so that we may cast the electromagnetic fields as

$$\mathbf{E}(x,y,z,t) = \mathbf{e}(x,y)\exp(i\beta z - i\omega t), \quad (1a)$$

$$\mathbf{H}(x,y,z,t) = \mathbf{h}(x,y)\exp(i\beta z - i\omega t), \quad (1b)$$

with  $\omega$  being the frequency of the monochromatic radiation. The homogeneity of the wavefield in the coordinate  $z$  is explicitly parameterized in terms of the propagation constant  $\beta$ . More specifically, we study TM waves where  $\mathbf{H}$  exists only onto planes parallel to the metal-dielectric interfaces, and therefore which component  $h_y$  vanishes. Later on we additionally consider wave confinement around the origin  $(x,y)=(0,0)$  in any given transverse plane.

The Maxwell's equations provide some relations between the transverse fields  $\mathbf{e}$  and  $\mathbf{h}$ . The electric field  $\mathbf{e}$  may be derived from  $\mathbf{h}$  by means of the equation  $\nabla \times \mathbf{H} = -i\omega\epsilon_0\epsilon\mathbf{E}$ , where  $\epsilon(y)$  is the relative dielectric constant of the foliar structure. Since the field vector is solenoidal we also find  $h_z = i\beta^{-1}\partial_x h_x$ ; therefore,  $h_x$  is the scalar wavefield from which we may describe the nondiffracting beam unambiguously. Let us point out that alternate routes for the description of electromagnetic diffraction-free beams may be found elsewhere [26–28].

The two-dimensional Helmholtz equation,

$$(\partial_x^2 + \partial_y^2 + \omega^2\epsilon/c^2 - \beta^2)h_x = 0, \quad (2)$$

may be of help in order to find any localized solution of the field  $h_x$ . In this study, however, an alternative approach is carried out. Based on the Bloch theorem [29], we may describe the propagating wavefield  $h_x$  as a superposition of Bloch modes having the form

$$h_x(x,y) = \sum_K \int_{-\infty}^{\infty} a_K h_K(y) \exp(ik_x x + iKy) dk_x, \quad (3)$$

where  $k_x$  is the (real) component of a wave vector along the  $x$ -axis and  $K$  is the so-called Bloch wave number, which generally is multivalued for a given  $k_x$ . Moreover,  $h_K(y+p) = h_K(y)$  is a periodic function, which is normalized as  $h_K(0)=1$  for convenience, and  $a_K$  is simply a field amplitude.

Assuming that sources are sufficiently far from the focal region of the localized beam, the role of evanescent waves [30] is negligible in our analysis and, therefore, they are disregarded setting  $a_K=0$  if  $\text{Im}(K) \neq 0$ . In this sense we also neglect material losses imposing that the relative dielectric constant of the medium is a real parameter of the problem [ $\text{Im}(\epsilon)=0$ ]. We point out that this is not strictly true in a realistic problem; plasma-like media with  $\epsilon < 0$  are necessarily dispersive since energy density considerations lead to the condition  $d(\omega\epsilon)/d\omega > 0$ , and the presence of dispersion in general signifies dissipation of energy [31]. However, it is possible to neglect the absorption in a transparency window where the imaginary part of  $\epsilon$  is very small in comparison with its real part.

In the case of the stratified medium shown in Fig. 1, the periodic function  $h_K = h_K^+ + h_K^-$  is conveniently written as the summation of two independent terms, being [32]

$$\begin{bmatrix} h_K^+ \\ h_K^- \end{bmatrix} = \exp(-iKy) \mathbf{T}_\alpha(y - y_\alpha) \begin{bmatrix} a_\alpha \\ b_\alpha \end{bmatrix}, \quad \text{for } y \in R_\alpha, \quad (4)$$

where  $\alpha$  is an integer that refers to a unique slab. Note that the amplitude  $a_\alpha$  is independent of  $a_K$  given in Eq. (3) and they should not be confused. The domains are  $R_\alpha \equiv (y_{\alpha-1}, y_\alpha]$ , where  $y_0=0, y_1=w$ , and  $y_{\alpha+2}=y_\alpha+p$ ; for instance,  $R_\alpha$  is associated with a region where the medium is metallic when  $\alpha$  is an odd number. In Eq. (4), the translation matrix is

$$\mathbf{T}_\alpha(y) = \begin{bmatrix} \exp(ik_{y\alpha}y) & 0 \\ 0 & \exp(-ik_{y\alpha}y) \end{bmatrix}. \quad (5)$$

Also,

$$k_{y\alpha} = \begin{cases} \sqrt{(\omega/c)^2 \epsilon_\alpha - k_\parallel^2}, & (\omega/c)^2 \epsilon_\alpha \geq k_\parallel^2 \\ i\sqrt{k_\parallel^2 - (\omega/c)^2 \epsilon_\alpha}, & (\omega/c)^2 \epsilon_\alpha < k_\parallel^2, \end{cases} \quad (6)$$

where  $\epsilon_1 = \epsilon_m$  and  $\epsilon_2 = \epsilon_d$  are the relative dielectric constants of the metallic medium and the dielectric material, respectively. For other slabs we use the recurrence relation  $\epsilon_{\alpha+2} = \epsilon_\alpha$ ; here  $\epsilon_\alpha$  at  $\alpha=0$  does not refer to its value in vacuum, but  $\epsilon_d$ . In Eq. (6) the real-valued wave vector onto a plane parallel to the metallo-dielectric interface has a squared modulus  $k_\parallel^2 = k_x^2 + \beta^2$ . Finally since material losses are neglected, the dielectric constants of the plasma-like material  $\epsilon_m < 0$  and that of the insulator  $\epsilon_d > 0$  are also real-valued parameters.

The continuities of the wavefield  $h_x$  and  $\epsilon^{-1} \partial_y h_x$  at the metallo-dielectric interfaces, together with the periodicity of  $h_K$ , determine the waveform of each Bloch mode and its dispersion behavior. Using the  $2 \times 2$  transfer matrix formulation for layered media [32] we may obtain the fields and the dispersion equation in a rather simple way. The latter explicitly reads

$$\begin{aligned} \cos(Kp) &= \cos[k_{yd}(p-w)] \cos(k_{ym}w) \\ &- \frac{(k_{ym}^2 \epsilon_d^2 + k_{yd}^2 \epsilon_m^2)}{2k_{yd}k_{ym}\epsilon_d\epsilon_m} \sin[k_{yd}(p-w)] \sin(k_{ym}w). \end{aligned} \quad (7)$$

In Fig. 2 we plot the real-valued  $K$  solutions of Eq. (7) for a multilayer medium composed of thin metallic films of width  $w=50$  nm, separated at a distance of  $p=450$  nm, and embedded in a dielectric medium of  $\epsilon_d=2.25$ . At a frequency of  $\omega=3.427$  fs<sup>-1</sup> (wavelength of  $\lambda_0=550$  nm in the vacuum) our plasma-like medium has a relative dielectric constant  $\epsilon_m=-15.0$ . A large bandgap in the interval  $k_\parallel p \in (0, 4.571)$  is followed by some two others in (5.126, 7.899) and (8.301, 8.503), together with the evanescent-wave regime at  $k_\parallel p > 8.737$ . As a consequence, real values of  $\beta$  are limited by  $\beta_{\max}=8.737/p$  in our example ( $\beta_{\max}=19.42$   $\mu\text{m}^{-1}$ ). This boundary value is reached at  $K = \pm \pi/p$  rather than at a zero value [33].

Let us point out that, if the superposition shown in Eq. (3) is such that  $k_\parallel$  is higher than the cutoff frequency

$$\beta_c = \sqrt{\epsilon_d} \omega/c, \quad (8)$$

occurring if  $k_\parallel p > 7.711$ , the wavefields are all of evanescent nature in the metal and in the dielectric; here  $\beta_c$

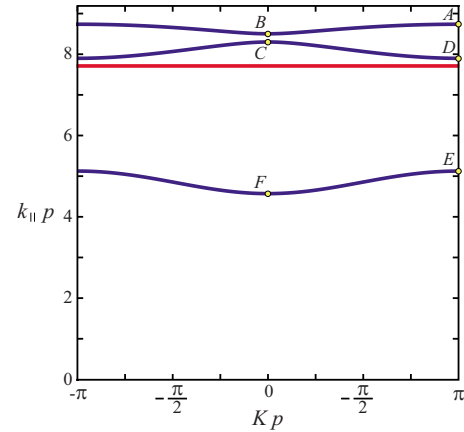


Fig. 2. (Color online) Dispersion equation at  $\omega=3.4 \times 10^{15}$  rad/s for a periodic media as presented in Fig. 1 with  $w=5 \times 10^{-8}$  m and  $p=4.5 \times 10^{-7}$  m. The red (straight) line marks the boundary of homogeneous- and evanescent-wave regimes in the dielectric,  $k_\parallel p=7.711$ . The points in yellow determine the cut-off normalized frequencies  $k_\parallel p$  of values (A) 8.737, (B) 8.503, (C) 8.301, (D) 7.899, (E) 5.126, and (F) 4.571.

$= 17.14$   $\mu\text{m}^{-1}$ . The cutoff frequency is plotted with a horizontal red line in Fig. 2. Interestingly, these evanescent waves may arise at values of  $k_\parallel p$  such that Eq. (7) gives a Bloch wave number with  $\text{Im}(K)=0$ . Thus, the evanescent waves are resonantly coupled leading to propagating Bloch-type constituents of the diffraction-free wavefield  $h_x(x, y)$ . Nondiffracting beams with a propagation constant  $\beta \in (\beta_c, \beta_{\max})$  are wavefields of this kind.

In Fig. 3 we map different contours of isofrequency  $\beta$  in the  $k_x K$  plane based on the graphical representation of the dispersion equation given in Fig. 2. The first band is presented in Fig. 3(a) providing a surface of maxima at  $k_x=0$  and  $K = \pm \pi/p$  reaching  $\beta_{\max}$ . Simple closed curves around these points are found for decreasing values of the propagation constant provided  $\beta_{c1} \leq \beta < \beta_{\max}$ , where  $\beta_{c1} p = 8.503$  coincides with the upper boundary of the first bandgap (point B in Fig. 2). At lower  $\beta$ , spatial frequencies around  $k_x=0$  cannot excite propagating Bloch modes leading to open (isofrequency) curves. This gap is re-

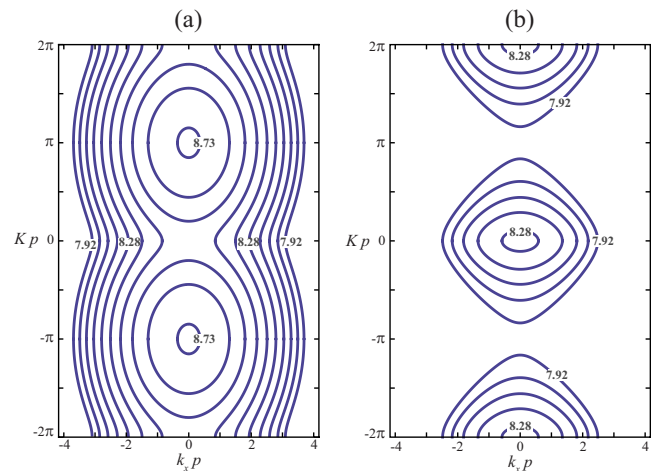


Fig. 3. (Color online) Isofrequency curves at different propagation constants  $\beta_c < \beta < \beta_{\max}$  are shown for the (a) first and (b) second sheets of the dispersion curve. Contour lines are labeled following the normalization  $\beta p$ .

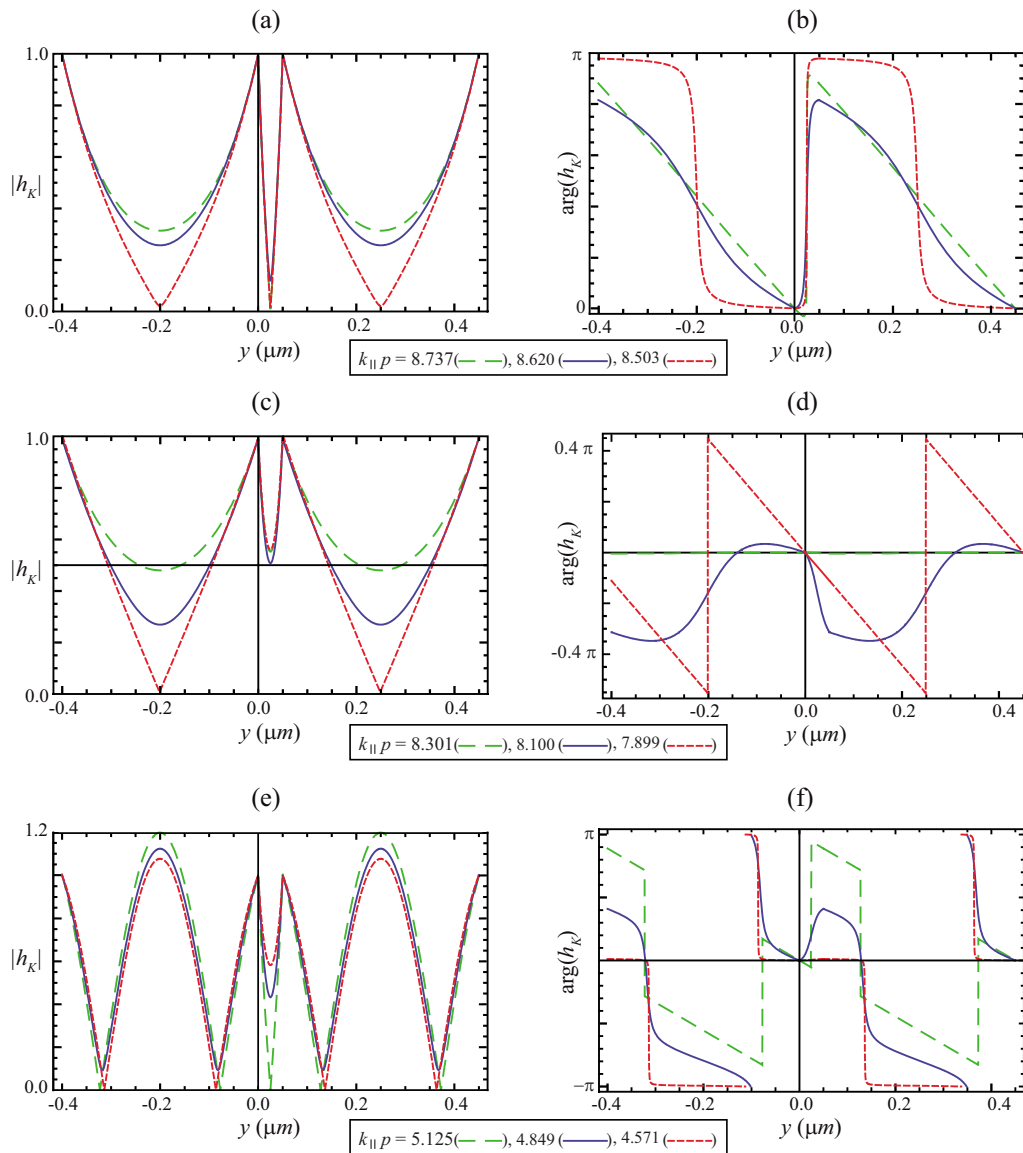


Fig. 4. (Color online) Behavior of the complex amplitude (left column) and argument (right column) of the wave function  $h_K$  at different values of  $k_{\parallel}$  and positive  $K$  corresponding to the first (top), second (middle), and third (bottom) bands.

moved in the second sheet of the dispersion equation, which arises for  $\beta \leq \beta_{c2}$  and it is shown in Fig. 3(b); obviously  $\beta_{c2}p = 8.301$  corresponds to the upper limit of the second band of allowed spatial frequencies  $k_{\parallel}$  (point C). In this case, the closed curves are centered at the origin of the plane  $k_x K$  (and at multiples of  $2\pi/p$  along the  $K$ -axis). Similarly to Fig. 3(a), the isofrequency curves are closed when  $\beta$  takes values belonging to the (second) band of allowed frequencies; here  $\beta_{c3} \leq \beta < \beta_{c2}$ , where  $\beta_{c3}p = 7.899$  (point D). Out of this interval, the isofrequency curves are open again.

To conclude, the periodic function  $h_K$  is depicted in Fig. 4 at different values of  $k_{\parallel}$ . In all cases, the absolute value  $|h_K|$  is an even function whereas its argument is an odd function with respect to the center of the metallic film, provided the latter is set off to zero (for instance, at  $y = w/2$ ). Peaks are formed at metal-dielectric interfaces and valleys are formed at the center of the slabs; this rule holds in the purely evanescent regime when  $k_{\parallel} > \beta_c$ . How-

ever the maximum of intensity is reached at the center of the dielectrics if  $k_{\parallel}$  belongs to the third band [see Fig. 4(e)]. On other hand we observe that phases of the wave function  $h_K$  have a characteristic variation at different spectral bands. For instance, phases are  $\sim \pi$  rad at the right side of the central metallic slab  $y = w$  in the top band; however, this phase turns to  $\sim 0$  in the second band. We show below that this is of relevance in the formation of an on-axis focus.

### 3. FOCUS GENERATION

Let us establish some favorable conditions for the formation of a focus along the  $z$ -axis. Using  $(x, y) = (0, 0)$  in Eq. (3) we obtain the wavefield amplitude  $h_x = \sum_K \int a_K dk_x$  at the origin as a summation of the amplitudes  $a_K$  corresponding to different Bloch modes. This may be interpreted as an interference of Bloch-type individuals. If the phase of their amplitudes is manipulated in order to have

the same value leading to in-phase waves, the oscillatory superposition yields the highest intensity achievable. Except a few particular conditions, it cannot find a point other than the origin from the  $xy$  plane where such a phase matching holds. As a consequence, a strong localization of the nondiffracting beam is expected to occur around the  $z$ -axis, with such a line unquestionably constituting a focus.

At this point of our analysis it is interesting to review the concept of focus wavefields in a system such as the uniform dielectric medium, where nondiffracting solutions of the wave equation are well known. Obviously we are speaking of Bessel beams [15]. Such a system would result from setting  $w=0$  in the layered medium of Fig. 1 to remove the metallic films from the dielectric host. In this case Eq. (7) leads trivially to the solutions  $K_{\pm} = \pm k_{yd}$ . Also  $h_K(y)=1$  in the whole  $xy$  plane. The phase matching condition at the origin is also observed over a radially symmetric transverse pattern if in addition  $a_K$  is in direct proportion to  $|d\phi/dk_x|=-1/K$ , where  $\phi$  is the polar angle in the  $k_x K$  plane. Thus inserting

$$a_{K_{\pm}} = \begin{cases} \frac{1}{\sqrt{\beta_c^2 - (k_x^2 + \beta^2)}}, & \text{if } |k_x| < \sqrt{\beta_c^2 - \beta^2} \\ 0, & \text{otherwise} \end{cases} \quad (9)$$

into Eq. (3) yields the Bessel wavefield  $h_x = 2\pi J_0(k_{\perp} r)$  provided  $\beta < \beta_c$  [see Eq. (8)], with

$$k_{\perp} = \sqrt{\beta_c^2 - \beta^2} \quad (10)$$

being the transverse wave number and  $r$  being the radial spatial coordinate (see [22] for further details). We point out that excitations of the type  $a_K=1/|K|$  [if  $\text{Im}(K)=0$ ,  $a_K=0$ , otherwise] also provide paraxial Bessel beams in periodic media [23] and in anisotropic crystals [34].

A field spectrum like that of Eq. (9) may be experimentally attained using an opaque screen, with a centered extremely thin transparent annulus placed at the front focal plane of a perfect lens [11]. Highly efficient approaches may be found using conical lenses [35,36] and mirrors [37], Fabry–Perot interferometers [14], leaky screens [38–40], and diffractive optical elements [41–43]. Using such devices as external sources in our system would excite the required diffraction-free wavefields in the layered medium. For simplicity we assume that the spectral strength of such nondiffracting beams has a form following Eq. (9),

$$a_K = \frac{1}{\sqrt{\gamma^2 - k_x^2}}, \quad \text{for } |k_x| < \gamma, \quad (11)$$

and  $a_K=0$  if  $|k_x| \geq \gamma$ .

Let us consider that  $\beta$  and  $\gamma$  may be tuned at convenience. Thus  $\beta \leq k_{\parallel} < \sqrt{\beta^2 + \gamma^2}$  so that we might apply any spectral band (i.e., ordinates in Fig. 2) arbitrarily. In our model it is reasonable to think of  $\sqrt{\beta^2 + \gamma^2}$  denoting the cutoff frequency  $\bar{\beta}_c = 2\pi\sqrt{\bar{\epsilon}_d}/\lambda_0$  associated with the uniform external medium of the dielectric constant  $\bar{\epsilon}_d$  where the source field is driven. In a great number of examples given below  $\bar{\beta}_c = \beta_{\max}$  yielding  $\bar{\epsilon}_d = 2.89$ ; in this medium the wavelength  $\bar{\lambda}_d = \lambda_0/\sqrt{\bar{\epsilon}_d} = 324$  nm and the minimum spot

size of the zero-order Bessel beam is  $(\Delta_x)_{\min} = 2.253/\gamma = 116$  nm where the maximum value of  $\gamma = \bar{\beta}_c$  at  $\beta=0$ . On the other hand, our model neglects filtering (apodizing) effects and aberrations on the wavefields induced at the boundaries of the system [22]. However, conventional techniques for its compensation might be employed in order to find a good agreement with our results. Otherwise the theory remains valid leaving the appropriate estimation of the spectrum  $a_K$ .

#### 4. SUBWAVELENGTH TRANSVERSE PATTERNS: NUMERICAL RESULTS

To illustrate the focus generation along the  $z$ -axis, we perform a numerical simulation in the periodic layered medium of  $p=450$  nm (and  $\epsilon_d=2.25$ ) with metallic films of  $w=50$  nm and  $\epsilon_m=-15.0$ . In Fig. 5 we show the field intensity  $|h_x|^2$  for a nondiffracting beam of propagation constant  $\beta=18.90 \mu\text{m}^{-1}$  ( $\beta=\beta_{c1}$ ), which spatial spectrum is given by Eq. (11) with  $\gamma=4.462 \mu\text{m}^{-1}$  ( $\gamma p=2.008$ ). Thus the maximum value of  $k_{\parallel}$  reaches a value coinciding with  $\beta_{\max}$ , i.e.,  $\beta_{c1} \leq k_{\parallel} < \beta_{\max}$  corresponding to the first band of allowed frequencies shown in Fig. 2. The isofrequency curve  $K=K(k_x)$  is also depicted in the inset of the figure, where excited frequencies  $k_x$  are shaded in blue. The intensity is maximum at the origin but the pattern exhibits no radial symmetry. The field distribution along the abscissa,

$$h_x(x, y=0) = 2 \int_{-\pi/2}^{\pi/2} \cos(\gamma x \cos \phi) d\phi = 2\pi J_0(\gamma x), \quad (12)$$

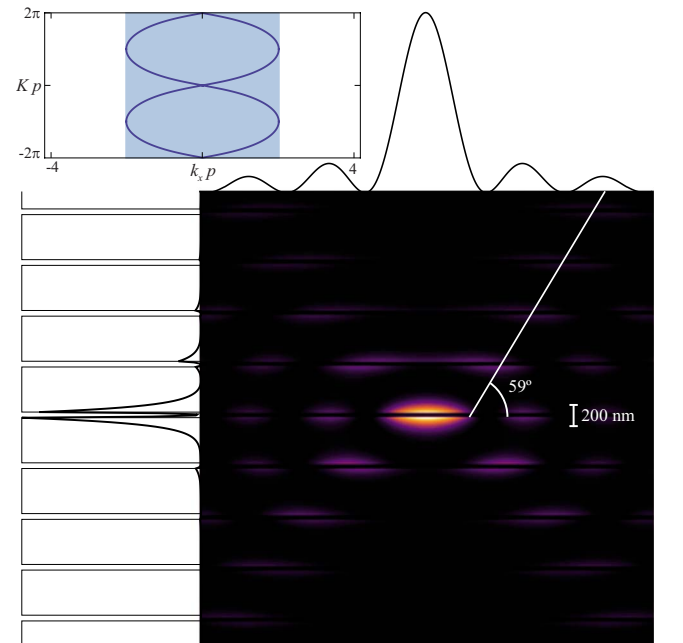


Fig. 5. (Color online) Contour plot of the intensity  $|h_x|^2$  in the  $xy$  plane corresponding to a localized diffraction-free beam of normalized propagation constant  $\beta p=8.503$  and transverse frequency  $\gamma p=2.008$  leading to  $(k_{\parallel p})_{\max}=8.737$ . Intensity distributions along the coordinate axes are shown at the top and left sides. Inset: Isofrequency curve where shaded region corresponds to the excited spatial bandwidth.

resembles that of the source field that would propagate in the homogeneous dielectric medium of  $\bar{\epsilon}_d=2.89$ . We point out that some discrepancies arise in Eq. (12) if some spatial frequencies  $k_x$  are excited but, because of the presence of a gap, they do not contribute to the resulting propagating wavefield; this case will be treated ahead. From Eq. (12) we derive that the full width at half-maximum (FWHM) of the intensity peak along this direction is inversely proportional to  $\gamma$  following  $\Delta_x=2.253/\gamma$ . In our case  $\Delta_x=505$  nm, which is above the wavelength in the dielectric host  $\lambda_d=\lambda_0/\sqrt{\epsilon_d}$  ( $=367$  nm). However, the behavior along the ordinate is significantly different. The most attractive feature of the wavefield is its high localization in the metal-dielectric interfaces, leading to fast decays when moving away from the surfaces and thus forming wedge-like shapes. This is in agreement with the patterns shown in Figs. 4(a) and 4(b) contributing to the integral (3) at  $x=0$ . Although the highest peak is attained at  $y=0$ , a large one also arises on the other side of the central metallic film,  $y=w$ . There, the Bloch modes  $h_K(y)\exp(iKy)$  are as strong as in focus and they interfere nearly in-phase (dephase  $<0.29\pi$  rad) giving a secondary focus. Ignoring this sidelobe, the FWHM of the figure is  $\Delta_y=45.99$  nm, well below  $\lambda_d$ .

Apart from surface resonances, radial asymmetry from focus is also attributed to a high concentration of light along certain directions in the  $xy$  plane. This directional enhancement of the radiated power may be explained by means of an effect coined as photon focusing [44], a term which was first used onto the strong anisotropy of heat flux in crystalline solids and that takes other names in optics like self-collimation [6], self-guiding [7], and subdiffractive propagation [45].

The estimation of the value(s) of the azimuthal coordinate  $\theta$  where photon focusing is manifested is based on the stationary-phase principle. First note that the phase factor  $\exp(ik_x x + iKy)$  of Eq. (3) varies rapidly when moving away from the origin,  $r \rightarrow \infty$ , being  $(x,y) = r(\cos \theta, \sin \theta)$ . This phase term also introduces strong oscillations for running  $k_x$  except in the vicinities of those spatial frequencies  $k_{xs}$  satisfying  $x + K'_s y = 0$ , where  $K' = dK/dk_x$  and the subindex  $s$  stands for the value given at  $k_{xs}$ . Setting  $K'_s = \tan \phi_s$  we have the solutions  $\phi_s = \theta \pm \pi/2$ ; consequently the tangent of the curve  $K(k_x)$  at the stationary points  $k_{xs}$  is normal to the vector position of the observation point  $(x,y)$ . Moreover, the asymptotic behavior of Eq. (3) depends exclusively on those stationary points  $k_{xs}$ ; substituting  $K$  by  $K_s$  in every term of the integrand, except the phase factor for which we use a quadratic expansion  $K \approx K_s + K'_s(k_x - k_{xs}) + K''_s(k_x - k_{xs})^2/2$ , finally yields

$$h_x(x,y) \approx \sum_{K,k_{xs}} a_K h_{K_s}(y) \exp(ik_{xs}x + iK_s y) I_{K_s}(y), \quad (13)$$

where

$$I_{K_s}(y) = \int_{-\infty}^{\infty} \exp[iK''_s(k_x - k_{xs})^2 y/2] dk_x = \sqrt{\frac{2\pi}{|K''_s y|}} \exp\left[i\frac{\pi}{4} \text{sgn}(K''_s y)\right]. \quad (14)$$

In this simple analysis we have also assumed that  $a_K$  has

a well behavior and it does not present discontinuities. In the far-field zone  $|h_x|^2$  decreases inversely proportional to the radial coordinate  $r$ , except those directions  $\theta$  where stationary points satisfy  $K''_s=0$ . In these cases the dispersion curve is flat leading to a significantly slow attenuation of the radiated power, at least much slower than  $r^{-1}$ .

In Fig. 6(a) we plot the solutions  $k_{xs}$  of the equation  $K''_s=0$  at different values of  $\beta$ . Considering that the dispersion (7) may be written as  $\cos(Kp) = f(k_x)$ , the solutions of the equation  $K''_s=0$  are also the frequencies  $k_{xs}$  satisfying

$$f''_s(1 - f_s^2) + f_s'^2 f_s = 0. \quad (15)$$

As shown in Fig. 3(a), the isofrequency curves for  $\beta_{c1} < \beta < \beta_{\max}$  mimic ellipses that lack of flat sections so that  $K''_s=0$  has no real solutions. For  $\beta = \beta_{c1}$ , the isofrequency curve presented also in the inset of Fig. 5 is flat at the origin of the plane  $k_x K$  taking a shape of X. In this case  $(k_{xs}, K_s) = (0,0)$  for which  $K'_s = \pm 0.604$  and  $\phi_s = \pm 31^\circ$ . See Fig. 6(b) showing the estimated (positive) values of  $\phi_s$  also for other propagation constants  $\beta$ . Our analysis concludes that the self-guiding phenomenon is expected at angles  $\theta = \pm 59^\circ$  (and  $\theta = \pm 121^\circ$ ), in agreement with the transverse pattern shown in Fig. 5. When  $\beta_{c3} < \beta < \beta_{c1}$ , solving Eq. (15) leads to increasing values of  $|k_{xs}|$  and therefore increasing values of  $|\phi_s|$  as shown in Figs. 6(a) and 6(b), respectively. Interestingly,  $k_{xs}=0$  becomes again a solution if  $\beta = \beta_{c3}$  (here giving  $K_s = \pm \pi/p$ ) for which  $\phi_s = \pm 42^\circ$ ; also  $k_{xs} = \pm 3.32/p$  gives  $K''_s=0$ , where  $\phi_s = \pm 73^\circ$ . Moreover, a minimum of four values of  $k_{xs}$  may be found for  $\beta < \beta_{c3}$  in which the zero-diffraction condition  $K''_s=0$  holds. We may conclude the general rule that a larger number of solutions come out when (positive)  $\beta$  decreases reaching new bandgaps for the frequency  $k_{\parallel}$  as shown in Fig. 2.

Let us analyze the intensity patterns of diffraction-free beams under the presence of bandgaps [ $\text{Im}(K) \neq 0$ ] within the source spectral window  $|k_x| < \gamma$ . In Fig. 7 we plot  $|h_x|^2$  of wavefields with the propagation constant  $\beta = \beta_{c3}$  corresponding to the lower limit of the second band. In Fig. 7(a)  $\gamma p = 2.552$  that yields  $(k_{\parallel})_{\max} = \beta_{c2}$ . This means that the source excites entirely the second band of allowed spatial frequencies with no gaps; therefore Eq. (12) is valid and  $\Delta_x = 2.253/\gamma$  ( $=397$  nm). Along the  $y$ -axis, the narrow peak around the origin has a FWHM of  $\Delta_y = 62.52$  nm and again is accompanied by a high sidelobe at the other side

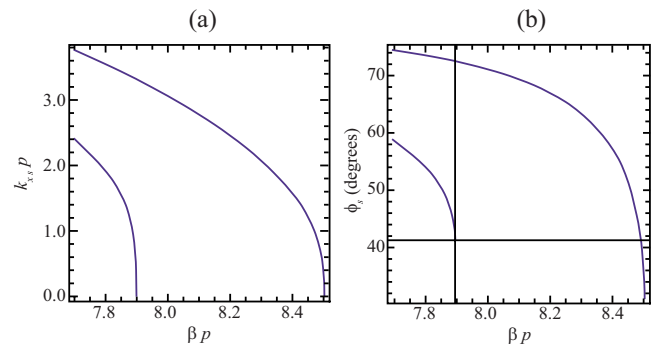


Fig. 6. (Color online) (a) Solutions  $k_x$  of Eq. (15),  $K''_s=0$ , associated with different propagation constants  $\beta$  of the wavefields, in the layered structure of Fig. 1. (b) Azimuthal angle  $\phi$  in the plane  $k_x K$  that corresponds to each solution of the aforementioned self-guiding condition.

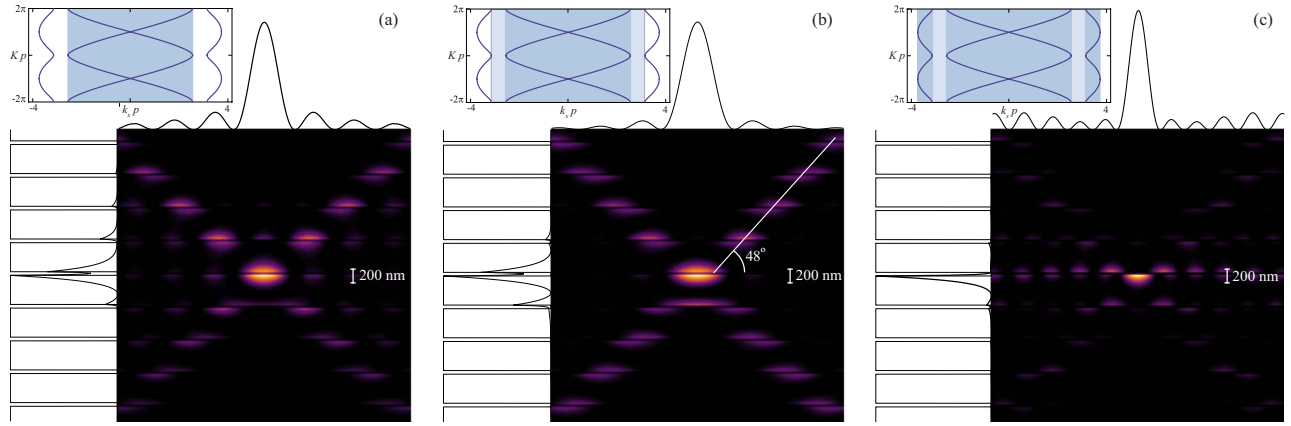


Fig. 7. (Color online) Transverse intensity  $|h_x|^2(x, y)$  for diffraction-free beams of  $\beta p = 7.899$  and spatial frequencies (a)  $\gamma p = 2.552$ , (b)  $\gamma p = 3.148$ , and (c)  $\gamma p = 3.734$ . Insets: Isofrequency curve at  $\beta p = 7.899$ . The blue shade indicates the spectral window in  $k_x$  under excitation. Light blue regions refer to gap-induced frustrated excitation.

of the metallic film. The formation of this secondary focus is again the constructive interference (nearly in-phase) of the Bloch modes from the second band. On other hand, self-collimation is attributed exclusively to the stationary points  $(k_{xs}, K_s) = (0, \pm \pi/p)$  giving  $\theta = \pm 48^\circ$  ( $\phi_s = \pm 42^\circ$  as seen above).

Setting  $\gamma p = 3.148$  as shown in Fig. 7(b), the bandgap  $\beta_{c2} < k_{\parallel} < \beta_{c1}$  is encountered, that is, frequencies satisfying  $\gamma_{c1} < |k_x| < \gamma_{c2}$  are frustratedly excited (being  $\gamma_{c1}p = 2.552$  and  $\gamma_{c2}p = 3.148$ ) so that the optical system behaves like a low-pass filter. In this case

$$h_x(x, y = 0) = 2\pi J_0(\gamma x) - h_{xc1}(\gamma x), \quad (16)$$

where

$$h_{xc1}(\gamma x) = 2 \int_{-\phi_{c1}}^{\phi_{c1}} \cos(\gamma x \cos \phi) d\phi = \sum_{m=0}^{\infty} C_m^{(c1)} J_{2m}(\gamma x), \quad (17)$$

with  $0 \leq \phi_{c1} < \pi/2$  such that  $\gamma \cos \phi_{c1} = \gamma_{c1}$ ,

$$C_m^{(c1)} = 4(-1)^m \frac{\sin(2m\phi_{c1})}{m}, \quad \text{for } m \neq 0, \quad (18)$$

and  $C_0^{(c1)} = 4\phi_{c1}$ . We point out that  $J_{2m}(0) = 0$  for  $m \neq 0$  so that in the vicinities of the focal point we have  $h_x \approx (2\pi - 4\phi_{c1})J_0(\gamma x)$ . However the central peak stretches slightly, specifically  $\Delta_x = 459$  nm, whereas sidelobes are altered significantly as expected. Moreover, the FWHM in the direction of the periodicity  $\Delta_y = 61.58$  nm and self-collimation angles  $\theta = \pm 48^\circ$  are also maintained in spite of bandgaps.

Finally, arriving at  $\gamma p = 3.734$  we are able to excite every allowed spatial frequency in the first band since  $(k_{\parallel})_{\max} = \beta_{\max}$ . The intensity  $|h_x|^2$  is depicted in Fig. 7(c) showing notable differences from the cases previously analyzed. For instance, the FWHM along the  $x$ -axis is  $\Delta_x = 277$  nm, which is close to the value we would obtain if we ignore the bandgap. In this case  $\Delta_x$  is lower than the radiation wavelength in the dielectric,  $\lambda_d = 367$  nm; however this subwavelength size is still higher than  $\lambda_d/2$  in the same order than a regular Bessel beam. Here we may evaluate the wavefield by

$$h_x(x, y = 0) = 2\pi J_0(\gamma x) - h_{xc1}(\gamma x) + h_{xc2}(\gamma x), \quad (19)$$

where  $\gamma \cos \phi_{c2} = \gamma_{c2}$ . Sidelobes are also strongly attenuated in all directions, even at those associated with self-collimation. Here  $\theta = \pm 48^\circ$  ( $\phi_s = \pm 42^\circ$ ) and also  $\theta = \pm 17^\circ$  ( $\phi_s = \pm 73^\circ$ ); as a consequence, sharing the power radiated in this large number of directions leads to the weakening of the photon-focusing effect. More importantly, the high sidelobe appearing previously in the  $y$ -axis seems to be wiped out completely. This effect may be explained considering that Bloch components from the first band and those from the second band are roughly out-of-phase at  $y = w$  [see Figs. 4(b) and 4(d)] so that they interfere destructively in Eq. (3). Additionally, the central peak is unaltered in practical terms, giving  $\Delta_y = 54$  nm.

## 5. HYBRID CONSTRUCTION OF DIFFRACTION-FREE WAVES

In the numerical simulations given above we have shown that beam sizes along the  $x$ -axis are larger than the diffraction limit  $\lambda_d/2$  attained by quasi-stationary Bessel beams propagating in the medium of the dielectric constant  $\epsilon_d$ , whereas  $\Delta_y$  is clearly subwavelength. Control over the wave pattern and thus over its FWHM in the  $x$  direction is exercised by the spectrum of spatial frequencies  $k_x$ : the higher is the bandwidth the lower is  $\Delta_x$ . From  $k_x^2 \leq \beta_{\max}^2 - \beta^2$  estimating the spectral domain of the wavefield we conclude that decreasing  $\beta$  leads to a widening of the spectrum. However, if  $\beta < \beta_c$  the plane-wave components in the dielectric material propagate homogeneously so that they are not necessarily coupled resonantly around the metal-dielectric surfaces. In principle, this effect might modify significantly the localization of the field in the direction of the periodicity. Let us clarify these aspects.

The contour plot shown in Fig. 8 corresponds to a diffraction-free beam of propagation constant  $\beta = 10.157 \mu\text{m}^{-1}$  ( $\beta p = 4.571$ ) coinciding with the lower limit of  $k_{\parallel}$  for the third band (see Fig. 2). The transverse frequency  $\gamma p = 7.446$  guarantees that all the three bands of allowed frequencies are excited; this is a high value since if it were generated in a uniform medium with  $\bar{\epsilon}_d = 2.89$  it

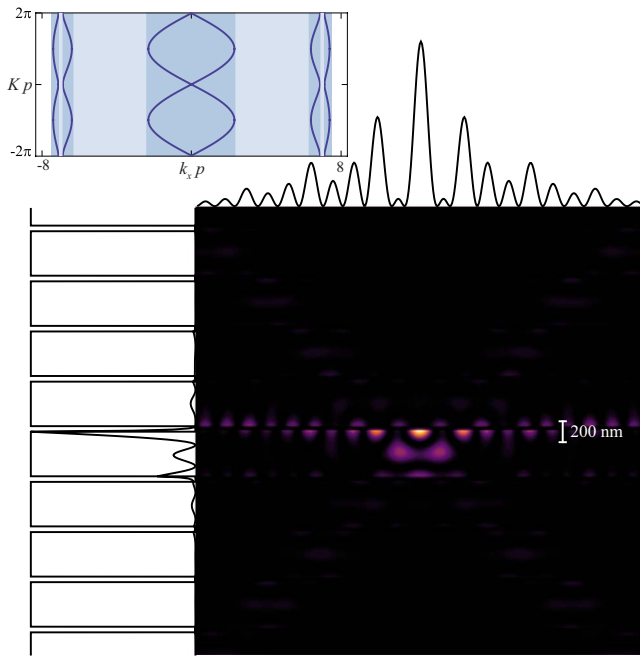


Fig. 8. (Color online) Intensity  $|h_x|^2$  in the transverse  $xy$  plane for a nondiffracting beam of  $\beta=10.16 \mu\text{m}^{-1}$  and  $\gamma=16.55 \mu\text{m}^{-1}$ . Excitation of Bloch modes with  $|k_x| < 5.15 \mu\text{m}^{-1}$  leads to nonevanescent wavelets in the dielectric slabs so that the resulting hybrid wavefield from Eq. (3) combines Bloch constituents of different nature.

would give a Bessel beam of width  $\Delta_x=136 \text{ nm}$ . Figure 8 shows that the intensity  $|h_x|^2$  is distributed mainly around the interface  $y=0$ . A narrow peak on the focus is produced exhibiting a width of  $\Delta_x=132 \text{ nm}$ , which is slightly lower than that just given above. Also strong side lobes arise in the vicinity of the focus. This suggests that bandgaps inherent in a photonic crystal provide a mechanism to achieve a superresolving effect going beyond the diffraction-induced Bessel limit. The origin of this superresolving effect is not the excitation of SPPs but an enhancement of high spatial frequencies [46].

On other hand, the field distribution in the  $y$ -axis demonstrates a subwavelength focus of FWHM  $\Delta_y=44 \text{ nm}$ . Side lobes on the interfaces are accompanied with other peaks in the middle of the dielectric slabs. This is not surprising since Bloch components of the third band shown in Fig. 4(e) and contributing in the expansion (3) have such a behavior. This effect is in fact more pronounced along directions oriented with polar angles  $\theta=\phi_s \pm \pi/2$ , with the stationary point being  $\phi_s=\pm 41^\circ$  ( $\theta=\pm 49^\circ$ ) associated with the self-collimation effect.

Although superresolution along the  $x$ -axis is modest in comparison with that obtained in the  $y$ -axis, we wonder if beam widths might surpass the diffraction limit in all directions. As resolved in Section 3, for our examples where  $\beta_{\text{max}}=19.42 \mu\text{m}^{-1}$  and  $\lambda_0=550 \text{ nm}$  this diffraction limit reads  $\Delta_{\text{min}}=116 \text{ nm}$ . In Fig. 9 we present the intensity distribution  $|h_x|^2$  of a nondiffracting beam excited with a transverse spatial frequency of  $\gamma=17.20 \mu\text{m}^{-1}$  giving a propagation constant of  $\beta=9.00 \mu\text{m}^{-1}$ . In this case the central peak is anamorphic and characterized by FWHMs of  $\Delta_x=109 \text{ nm}$  and  $\Delta_y=46 \text{ nm}$  all below the diffraction limit. The bandgap-induced filtering also leads to intense

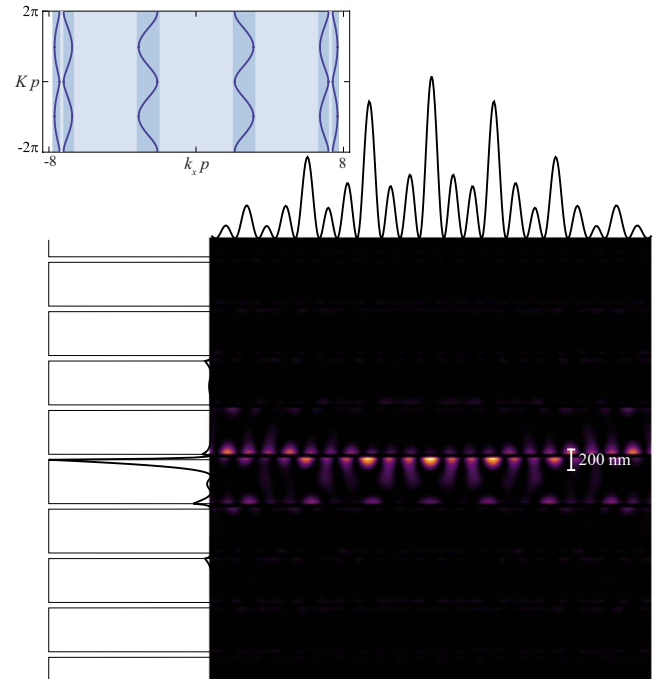


Fig. 9. (Color online) Transverse pattern of a nondiffracting beam with  $\beta=9.00 \mu\text{m}^{-1}$ . The beam width of the main central focus has  $\Delta_x=109 \text{ nm}$  and  $\Delta_y=46 \text{ nm}$ , going beyond the diffraction limit  $\Delta_{\text{min}}=116 \text{ nm}$ .

side lobes along the interface  $y=0$ ; however they decay as going beyond the focus. Moreover, the peak intensity of these secondary foci cannot exceed the intensity of the main focus.

## 6. EXTREME LOCALIZATION

The central spot size of the nondiffracting beam is fundamentally limited by the maximum value achievable by  $k_{\parallel}$ . Taking into account that  $k_{\parallel} \leq \beta_{\text{max}}$ , large values may be reached by using materials with high refractive indices. Also, the geometry of the layered structure has a great impact upon  $\beta_{\text{max}}$ , which may be tuned by modifying the widths  $w$  of the metallic layers and that of the dielectric layers,  $p-w$ . This is clearly seen within the effective medium theory. Assuming that  $p \ll \lambda_0$ , Eq. (7) approaches an ellipsoid of revolution [47]. The  $p$ -polarized waves thus are formally analogous to the so-called extraordinary waves in a uniaxial crystal. As a consequence, the modulus of the wave vector projected onto the  $xz$  plane would take a maximum value given by  $\beta_{\text{max}} = \sqrt{\epsilon_{\text{eff}}}\omega/c$ , where the effective permittivity  $\epsilon_{\text{eff}}$  for the extraordinary waves satisfies the equation

$$\frac{1}{\epsilon_{\text{eff}}} = \frac{w}{p} \frac{1}{\epsilon_m} + \frac{p-w}{p} \frac{1}{\epsilon_d}. \quad (20)$$

The value of  $\beta_{\text{max}}$  might be infinitely large in the case  $\epsilon_{\text{eff}} \rightarrow \infty$ , which occurs if

$$\frac{p}{w} = 1 - \frac{\epsilon_d}{\epsilon_m}. \quad (21)$$

Introducing Eq. (21) into the dispersion (7) one may observe that  $k_{\parallel}$  is bounded, however, reaching values extremely higher than  $\omega/c$ .

Figure 10 shows the transverse intensity  $|h_x|^2$  of a non-diffracting beam propagating in a layered medium of period  $p=13.2$  nm made of a metallic ( $\epsilon_m=-12.9$ ) and a dielectric ( $\epsilon_d=13.9$ ) material. Equation (21) provides the width  $w=6.35$  nm of the metallic films. The propagation constant  $\beta$  is arbitrary chosen; let us make it coinciding with the wave number of a plane wave propagating in vacuum,  $\omega/c=11.4 \mu\text{m}^{-1}$ . This is much lower than the maximum value attainable,  $\beta_{\text{max}}=595 \mu\text{m}^{-1}$ . Note that the environment medium necessary to excite wavefields with  $k_{\parallel}$  of such a magnitude requires an index of refraction higher than  $\sqrt{\epsilon_d}=52$ , which is dramatically large for dielectric materials in the visible spectrum. This suggests that external sources should launch nondiffracting beams of evanescent nature [48,49]. Also Eq. (7) gives a single-band isofrequency curve leading to the Bessel pattern in the form of Eq. (12) along the  $x$ -axis. In this case, a highly subwavelength FWHM of the central spot is achieved,  $\Delta_x=3.79$  nm, due to the fact that  $\gamma \lesssim \beta_{\text{max}}$ . In the perpendicular direction the FWHM is still lower giving  $\Delta_y=2.05$  nm. Finally, the transverse diffraction pattern is blurred along the  $y$ -axis caused by the eccentricity of the elliptical isofrequency curve.

The nano-layered periodic structure employed in Fig. 10 has also an attractive property not mentioned yet. The isofrequency curves are nearly flat within the range  $|k_x|p \leq 1$ . In our case  $p \ll \lambda_0$  leading to a self-collimation regime that is extended over a large spatial bandwidth. Excitation of a Bessel beam with a propagation constant of  $\beta=9.00 \mu\text{m}^{-1}$  and a transverse spectral width of  $\gamma=17.20 \mu\text{m}^{-1}$ , as performed in Fig. 9, would lead to the formation of Bloch waves in the periodic medium with the same Bloch wave number  $K=11.9 \mu\text{m}^{-1}$ . The result is shown in Fig. 11. The Bessel profile along the  $x$ -axis has a FWHM of  $\Delta_x=131$  nm, slightly higher than that observed in Fig. 9; on other hand, it exhibits lower sidelobes. Fur-

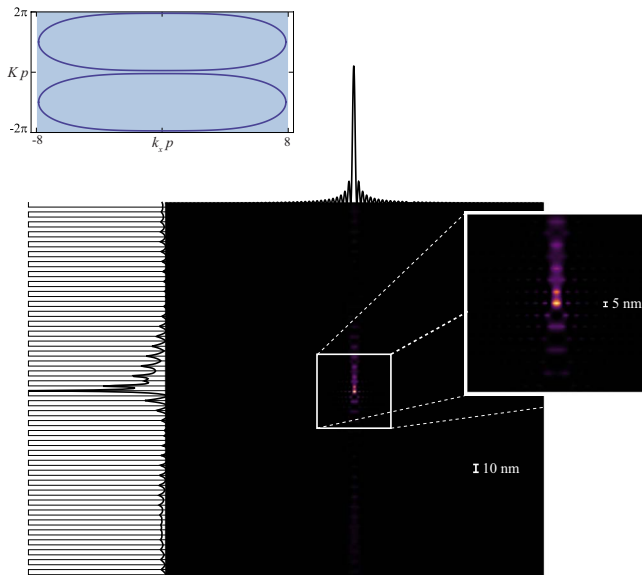


Fig. 10. (Color online) Transverse intensity  $|h_x|^2$  of a diffraction-free beam traveling in a metal-dielectric multilayer of period  $p=13.2$  nm. The propagation constant  $\beta=11.4 \mu\text{m}^{-1}$  is significantly lower than the maximum value achievable,  $\beta_{\text{max}}=595 \mu\text{m}^{-1}$ , leading to extreme subwavelength localization.

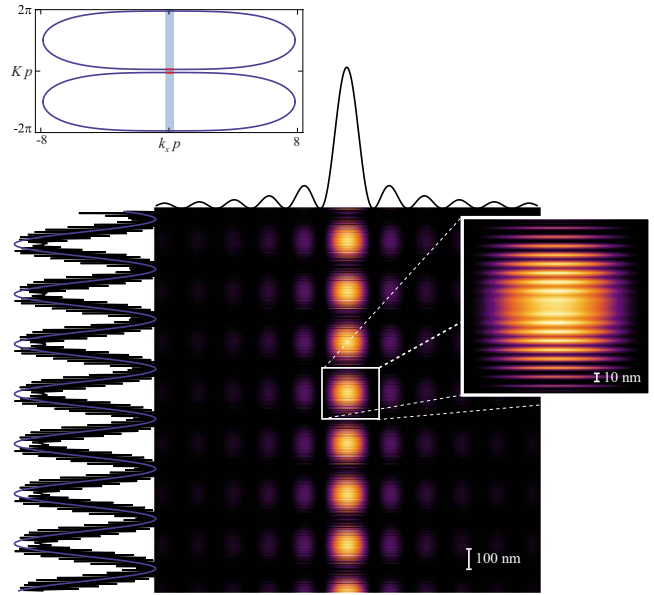


Fig. 11. (Color online) Intensity pattern in the  $xy$  plane corresponding to a nondiffracting beam of propagation constant  $\beta=9.00 \mu\text{m}^{-1}$  and transverse frequency  $\gamma=17.20 \mu\text{m}^{-1}$ . The planar isofrequency curve induces a self-guiding effect along the  $y$ -axis providing Bloch waves with  $K=11.9 \mu\text{m}^{-1}$ . Interference fringes are caused by counter-propagating wave functions.

thermore, the field pattern in the  $y$ -axis presents enormous differences in comparison with numerical simulations given above. Wave localization in the metal-dielectric surfaces seems to be uniformly distributed except for a long-period modulation. The flat dispersion curve induces a focus generation with an infinitely large depth of field [11], thus preventing from light concentration around a single interface. Also interference of counter-propagating Bloch waves featuring the formation of the transverse focus [22] leads to the production of Young-type fringes with an intensity variation of the envelope [blue solid line in Fig. 11] that is proportional to  $\cos^2(Ky)$ . Thus the envelope of these standing Bloch waves shows equienergetic peaks, which FWHM yields  $\Delta_y=132$  nm.

It is interesting to mention that well-shaped foci might be formed in the absence of back-propagating waves [22]. In such a case the intensity pattern depicted in Fig. 11 would conserve the Besselian shape along the  $x$ -axis. On the contrary it would leave a full wave delocalization upon the spatial coordinates  $y$  and  $z$ . As discussed previously, invariant propagation along these two orientations has a distinct origin. One is caused by the flattening of the isofrequency curve, and the other is produced by an external filtering leaving plane-wave constituents of the wavefield developing the same phase velocity projected along the  $z$ -axis.

## 7. CONCLUDING REMARKS

We have demonstrated that diffraction-free beams propagating in structured media composed of alternating layers of positive and negative  $\epsilon$ 's may reach beam sizes surpassing the diffraction limit. The periodic medium may exhibit positive, negative, and even plane isofrequency

curves since it is not responsible for the self-collimation phenomenon. Instead the nondiffracting effect lies on the spatial characteristics of the beam itself. We demonstrate that both are not self-exclusory mechanisms and therefore they may be introduced simultaneously along two perpendicular directions.

For an excitation of the form given in Eq. (11), we recall that the diffraction limit is attained when the transverse spatial frequency is maximum,  $\gamma_{\max} = \sqrt{\epsilon_d} \omega / c$ , leading to stationary ( $\beta=0$ ) Bessel waves with a central spot of FWHM  $\Delta_{\min} = 2.253 / \gamma_{\max}$ . In the layered system, two different mechanisms lead to the superresolving effect. A bandpass filtering due to the existence of gaps in the spatial spectrum of  $k_x$  modifies the response of the system transversally providing a narrow peak along the  $x$ -axis with moderate gain ( $\Delta_x \leq \Delta_{\min}$ ) and high sidelobes (secondary foci). In the direction of the periodicity, however, superresolution is carried out by the formation of surface resonances in the metal-dielectric interfaces leading to fast decays out of these planes. In our numerical simulations,  $\Delta_y$  can be as low as a third of  $\Delta_{\min}$ . Additionally, dephasing of Bloch constituents belonging to different bands contributes to the growth control of secondary foci in nearby surfaces.

In principle, subwavelength beam widths along an infinitely long distance might potentially be obtained. However practical limitations in the geometry of the system leads to the generation of invariant wavefields along with a finite axial distance. The estimation of such limits is similar, for example, to that corresponding to Bessel beams propagating in free space [15,16], and therefore they are not discussed here. However we point out the decisive role of the structured medium in order to achieve the subwavelength beam sizes: these wavefields cannot be sustained in free space for ranges longer than a wavelength. Relevant aspects in near-field subwavelength nondiffracting beams are exhaustively investigated by Kukhlevsky and co-workers [49–52].

Finally, material losses are neglected in our analysis. Since  $\text{Im } \epsilon \neq 0$  leads to wave damping in an unbounded dissipative system, absorption in the medium should be accounted for assuming a limited number of slabs. We have performed numerical simulations showing that the superresolving effect along the  $y$ -axis is practically maintained for a small absorption coefficient of the metallic medium and a moderate number of layers, whereas the peak slightly gets wider along the  $x$ -axis. Even when assuming that the focus is placed at an interface near the center of the system, boundary effects and also tunneling effects cannot be ignored. For instance, setting  $\epsilon_m = -15 + i0.15$  we may excite a diffraction-free beam with a propagation constant of  $\beta = 9 \mu\text{m}^{-1}$  and a central peak of  $\Delta_x = 139 \text{ nm}$  and  $\Delta_y = 43 \text{ nm}$  in a medium composed of 20 unit cells. The deterioration in the resolution power along the  $x$ -axis is mainly caused by a selective increment in  $\text{Im } K$  within the allowed spectral bands, an effect that is especially dramatic in the highest band. We have estimated that the central peak is also enlarged to a lesser extent by increasing the number of layers. Under these unfavorable conditions the beam size is still surpassing the diffraction limit along the direction of the periodicity. On other hand, a significant attenuation of the focal in-

tensity is also evident. In our numerical simulation, in-focus intensity decreases down to 18% (6%) from its original value if  $\text{Im } \epsilon_m = 0.15$  and the number of unit cells is 10 (20). A paper containing an extended analysis with further details is in preparation.

## ACKNOWLEDGMENTS

The authors are grateful to an anonymous reviewer for detailed and valuable comments. This research was funded by the Ministerio de Ciencia e Innovación (MICIIN) under the project TEC2009-11635.

## REFERENCES

1. A. E. Siegman, *Lasers* (University Science Books, 1986).
2. D. G. Grier, "A revolution in optical manipulation," *Nature* **424**, 810–816 (2003).
3. B. Hafizi, E. Esarey, and P. Sprangle, "Laser-driven acceleration with Bessel beams," *Phys. Rev. E* **55**, 3539–3545 (1997).
4. Z.-Y. Li and L.-L. Lin, "Evaluation of lensing in photonic crystal slabs exhibiting negative refraction," *Phys. Rev. B* **68**, 245110 (2003).
5. R. W. Ziolkowski, "Localized transmission of electromagnetic energy," *Phys. Rev. A* **39**, 2005–2033 (1989).
6. H. Kosaka, T. Kawashima, A. Tomita, M. Notomi, T. Tamamura, T. Sato, and S. Kawakami, "Self-collimating phenomena in photonic crystals," *Appl. Phys. Lett.* **74**, 1212–1214 (1999).
7. D. N. Chigrin, S. Enoch, C. M. Sotomayor-Torres, and G. Tayeb, "Self-guiding in two-dimensional photonic crystals," *Opt. Express* **11**, 1203–1211 (2003).
8. K. Staliunas and R. Herrero, "Nondiffractive propagation of light in photonic crystals," *Phys. Rev. E* **73**, 016601 (2006).
9. P. T. Rakich, M. S. Dahlem, S. Tandon, M. Ibanescu, M. Soljacic, G. S. Petrich, J. D. Joannopoulos, L. A. Kolodziejski, and E. P. Ippen, "Achieving centimetre-scale supercollimation in a large-area two-dimensional photonic crystal," *Nature Mater.* **5**, 93–96 (2006).
10. Z. Lu, S. Shi, J. A. Murakowski, G. J. Schneider, C. A. Schuetz, and D. W. Prather, "Experimental demonstration of self-collimation inside a three-dimensional photonic crystal," *Phys. Rev. Lett.* **96**, 173902 (2006).
11. G. Indebetouw, "Nondiffracting optical fields: some remarks on their analysis and synthesis," *J. Opt. Soc. Am. A* **6**, 150–152 (1989).
12. J. Fagerholm, A. T. Friberg, J. Huttunen, D. P. Morgan, and M. M. Salomaa, "Angular-spectrum representation of nondiffracting X waves," *Phys. Rev. E* **54**, 4347–4352 (1996).
13. J. H. McLeod, "The axicon: a new type of optical element," *J. Opt. Soc. Am.* **44**, 592–596 (1954).
14. Z. L. Horváth, M. Erdélyi, G. Szabó, Z. Bor, F. K. Tittel, and J. R. Cavallaro, "Generation of nearly nondiffracting Bessel beams with a Fabry–Perot interferometer," *J. Opt. Soc. Am. A* **14**, 3009–3013 (1997).
15. J. Durnin, "Exact solutions for nondiffracting beams. I. The scalar theory," *J. Opt. Soc. Am. A* **4**, 651–654 (1987).
16. J. Durnin, J. J. Miceli, and J. H. Eberly, "Diffraction-free beams," *Phys. Rev. Lett.* **58**, 1499–1501 (1987).
17. H. E. Hernández-Figueroa, M. Zamboni-Rached, and E. Recami, eds., *Localized Waves* (Wiley, 2008).
18. D. Mugnai, A. Ranfagni, and R. Ruggeri, "Observation of superluminal behaviors in wave propagation," *Phys. Rev. Lett.* **84**, 4830–4833 (2000).
19. S. Longhi, K. Janner, and P. Laporta, "Propagating pulsed Bessel beams in periodic media," *J. Opt. B: Quantum Semi-classical Opt.* **6**, 477–481 (2004).
20. A. V. Novitsky and D. V. Novitsky, "Nondiffracting electromagnetic fields in inhomogeneous isotropic media," *J. Phys. A* **39**, 5227–5231 (2006).

21. C. J. Zapata-Rodríguez, M. A. Porras, and J. J. Miret, "Free-space delay lines and resonances with ultraslow pulsed Bessel beams," *J. Opt. Soc. Am. A* **25**, 2758–2763 (2008).
22. C. J. Zapata-Rodríguez and J. J. Miret, "Diffraction-free beams in thin films," *J. Opt. Soc. Am. A* **27**, 663–670 (2010).
23. J. J. Miret and C. J. Zapata-Rodríguez, "Diffraction-free beams with elliptic Bessel envelope in periodic media," *J. Opt. Soc. Am. B* **25**, 1–6 (2008).
24. D. N. Christodoulides, F. Lederer, and Y. Silberberg, "Discretizing light behaviour in linear and nonlinear waveguide lattices," *Nature* **424**, 817–823 (2003).
25. O. Manela, M. Segev, and D. N. Christodoulides, "Nondiffracting beams in periodic media," *Opt. Lett.* **30**, 2611–2613 (2005).
26. Z. Bouchal and M. Olivik, "Non-diffracting vector Bessel beams," *J. Mod. Opt.* **42**, 1555–1566 (1995).
27. Z. Bouchal, J. Bajér, and M. Bertolotti, "Vectorial spectral analysis of the nonstationary electromagnetic field," *J. Opt. Soc. Am. A* **15**, 2172–2181 (1998).
28. P. Pääkkönen, J. Tervo, P. Vahimaa, J. Turunen, and F. Gori, "General vectorial decomposition of electromagnetic fields with application to propagation-invariant and rotating fields," *Opt. Express* **10**, 949–959 (2002).
29. J. D. Joannopoulos, S. G. Johnson, J. N. Winn, and R. D. Meade, *Photonic Crystals: Molding the Flow of Light* (Princeton U. Press, 2008).
30. S. A. Ramakrishna and O. J. F. Martin, "Resolving the wave vector in negative refractive index media," *Opt. Lett.* **30**, 2626–2628 (2005).
31. L. D. Landau, E. M. Lifshitz, and L. P. Pitaevskii, *Electrodynamics of Continuous Media* (Butterworth-Heinemann, 1984).
32. P. Yeh, *Optical Waves in Layered Media* (Wiley, 1988).
33. V. Kuzmiak and A. A. Maradudin, "Photonic band structures of one- and two-dimensional periodic systems with metallic components in the presence of dissipation," *Phys. Rev. B* **55**, 7427–7444 (1997).
34. A. Ciattoni and C. Palma, "Nondiffracting beams in uniaxial media propagating orthogonally to the optical axis," *Opt. Commun.* **224**, 175–183 (2003).
35. R. Grunwald, U. Griebner, F. Tschirschwitz, E. T. J. Nibbering, T. Elsaesser, V. Kebbel, H.-J. Hartmann, and W. Jüptner, "Generation of femtosecond Bessel beams with microaxicon arrays," *Opt. Lett.* **25**, 981–983 (2000).
36. C. J. Zapata-Rodríguez and A. Sánchez-Losa, "Three-dimensional field distribution in the focal region of low-Fresnel-number axicons," *J. Opt. Soc. Am. A* **23**, 3016–3026 (2006).
37. K. B. Kuntz, B. Braverman, S. H. Youn, M. Lobino, E. M. Pessina, and A. I. Lvovsky, "Spatial and temporal characterization of a Bessel beam produced using a conical mirror," *Phys. Rev. A* **79**, 043802 (2009).
38. S. Holm, "Bessel and conical beams and approximation with annular arrays," *IEEE Trans. Ultrason. Ferroelectr. Freq. Control* **45**, 712–718 (1998).
39. K. Reivelt and P. Saari, "Optically realizable localized wave solutions of the homogeneous scalar wave equation," *Phys. Rev. E* **65**, 046622 (2002).
40. K. Reivelt and P. Saari, "Experimental demonstration of realizability of optical focus wave modes," *Phys. Rev. E* **66**, 056611 (2002).
41. A. Vasara, J. Turunen, and A. T. Friberg, "Realization of general nondiffracting beams with computer-generated holograms," *J. Opt. Soc. Am. A* **6**, 1748–1754 (1989).
42. J. Amako, D. Sawaki, and E. Fujii, "Microstructuring transparent materials by use of nondiffracting ultrashort pulse beams generated by diffractive optics," *J. Opt. Soc. Am. B* **20**, 2562–2568 (2003).
43. Z. Li, K. B. Alici, H. Caglayan, and E. Ozbay, "Generation of an axially asymmetric Bessel-like beam from a metallic subwavelength aperture," *Phys. Rev. Lett.* **102**, 143901 (2009).
44. D. N. Chigrin, "Radiation pattern of a classical dipole in a photonic crystal: Photon focusing," *Phys. Rev. E* **70**, 056611 (2004).
45. K. Staliunas, C. Serrat, R. Herrero, C. Cojocar, and J. Trull, "Subdiffractive light pulses in photonic crystals," *Phys. Rev. E* **74**, 016605 (2006).
46. M. Martínez-Corral, P. Andrés, C. J. Zapata-Rodríguez, and M. Kowalczyk, "Three-dimensional superresolution by annular binary filters," *Opt. Commun.* **165**, 267–278 (1999).
47. A. Yariv and P. Yeh, "Electromagnetic propagation in periodic stratified media. II. Birefringence, phase matching, and x-ray lasers," *J. Opt. Soc. Am.* **67**, 438–448 (1977).
48. S. Ruschin and A. Leizer, "Evanescent Bessel beams," *J. Opt. Soc. Am. A* **15**, 1139–1143 (1998).
49. S. V. Kuchlevsky and M. Mechler, "Diffraction-free subwavelength-beam optics at nanometer scale," *Opt. Commun.* **231**, 35–43 (2004).
50. S. V. Kuchlevsky, M. Mechler, L. Csapo, and K. Janssens, "Near-field diffraction of fs and sub-fs pulses: super resolution of nsom in space and time," *Phys. Lett. A* **319**, 439–447 (2003).
51. S. V. Kuchlevsky, M. Mechler, L. Csapó, K. Janssens, and O. Samek, "Enhanced transmission versus localization of a light pulse by a subwavelength metal slit," *Phys. Rev. B* **70**, 195428 (2004).
52. G. Nyitrai, V. Mathew, and S. V. Kuchlevsky, "Generation and interference collapse of distortion-less fs pulses in free space by Fresnel sources," *Opt. Commun.* **281**, 1082–1086 (2008).